Journal of Power Sources 256 (2014) 52–60

Contents lists available at ScienceDirect

Journal of Power Sources

journal homepage: www.elsevier.com/locate/jpowsour

Multi-layer thin-film electrolytes for metal supported solid oxide fuel cells

Markus Haydn [a,*], Kai Ortner [b], Thomas Franco [a], Sven Uhlenbruck [c], Norbert H. Menzler [c], Detlev Stöver [c], Günter Bräuer [b], Andreas Venskutonis [a], Lorenz S. Sigl [a], Hans-Peter Buchkremer [c], Robert Vaßen [c]

[a] Plansee SE, 6600 Reutte, Austria
[b] Fraunhofer Institute for Surface Engineering and Thin Films, Bienroder Weg 54 E, 38108 Braunschweig, Germany
[c] Forschungszentrum Jülich, Institute of Energy and Climate Research (IEK), Wilhelm-Johnen-Straße, 52428 Jülich, Germany

HIGHLIGHTS

- Metal-supported solid oxide fuel cells for mobile applications.
- Development of multi-layer electrolytes by means of gas-flow sputtering process.
- First electrochemical cell tests show current densities higher than 2 A cm^{-2} at 0.7 V and 850 °C.

ARTICLE INFO

Article history:
Received 30 September 2013
Received in revised form
18 December 2013
Accepted 1 January 2014
Available online 18 January 2014

Keywords:
Solid oxide fuel cell
Metal-supported cell
Electrolyte
Gas-flow sputtering

ABSTRACT

A key to the development of metal-supported solid oxide fuel cells (MSCs) is the manufacturing of gas-tight thin-film electrolytes, which separate the cathode from the anode. This paper focuses the electrolyte manufacturing on the basis of 8YSZ (8 mol.-% Y_2O_3 stabilized ZrO_2). The electrolyte layers are applied by a physical vapor deposition (PVD) gas flow sputtering (GFS) process. The gas-tightness of the electrolyte is significantly improved when sequential oxidic and metallic thin-film multi-layers are deposited, which interrupt the columnar grain structure of single-layer electrolytes. Such electrolytes with two or eight oxide/metal layers and a total thickness of about 4 μm obtain leakage rates of less than 3×10^{-4} hPa dm^3 s^{-1} cm^{-2} (Δp: 100 hPa) at room temperature and therefore fulfill the gas tightness requirements. They are also highly tolerant with respect to surface flaws and particulate impurities which can be present on the graded anode underground. MSC cell tests with double-layer and multilayer electrolytes feature high power densities more than 1.4 W cm^{-2} at 850 °C and underline the high potential of MSC cells.

1. Introduction

Over the last decades, global development and industrializing activities in the field of solid oxide fuel cells (SOFCs) were dominated by two cell technologies, i.e. the anode-supported (ASC) and the electrolyte-supported (ESC) cell. Both cell types have demonstrated highly efficient power generation and cost effective cell manufacturing by using well established ceramic processing technologies such as screen printing and tape casting [1]. Supported by high development efforts, SOFC systems are currently giving their debut in commercial markets, e.g. in stationary power and/or combined heat and power (CHP) applications [2,3].

Besides stationary applications, the interest for mobile and portable power generation has been growing continuously during the past years [12]. SOFC system requirements for such applications being very challenging, e.g. frequent redox- and thermo-cycles as well as short start-up times. It was readily realized that ceramic ASC and ESC technologies do not fully suffice the demands. To meet this challenge, developments to create SOFCs based on a metal-supported cell (MSC) technology were initiated [4–11]. Reinforced by a metallic support, an MSC combines significantly improved mechanical stability with a much enhanced thermal and redox behavior as compared to fully ceramic cell systems, and thus addresses all important requirements for mobile applications.

* Corresponding author. Tel.: +43 5672 600 2007; fax: +43 5672 600 563.
E-mail address: markus.haydn@plansee.com (M. Haydn).

0378-7753/$ – see front matter © 2014 Elsevier B.V. All rights reserved.
http://dx.doi.org/10.1016/j.jpowsour.2014.01.043

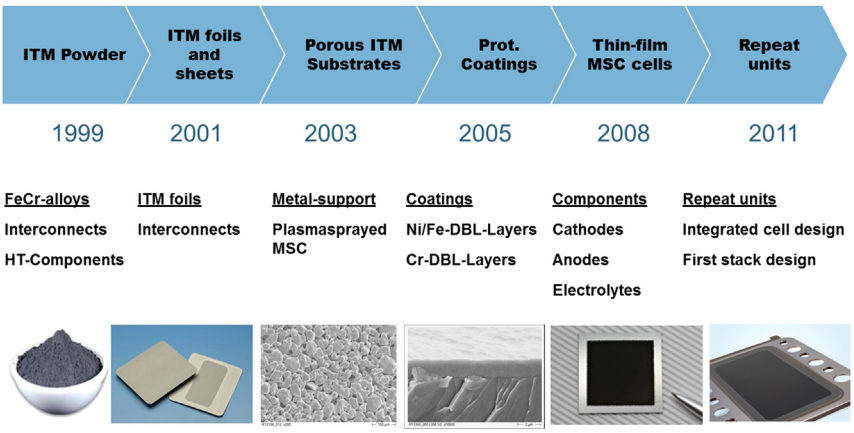

Fig. 1. Milestones of MSC development.

Plansee's activities in the field of component development for the MSC date back to the 1990s. At that time, a ferrite oxide dispersion strengthened Fe–Cr-alloy (trade name ITM) was developed which enables the fabrication of a porous metallic support within a powder-metallurgical (P/M) manufacturing route. This porous ITM substrate can be seen as an outstanding component – as a "backbone" of the whole MSC. Principally, it allows the set-up of thin ceramic cell layers and hence the fabrication of a high performance thin-film MSC. Moreover, this substrate has a strong contribution to the requirements of a mobile cell concept as already mentioned above.

Further milestones of component development are shown in Fig. 1. Due to a manifoldness of detailed cell component development, which has been performed in strong cooperation with Forschungszentrum Jülich (Jülich), the Karlsruhe Institute of Technology (KIT), and the Fraunhofer Institute for Surface Engineering and Thin Films, respectively, a novel MSC concept for mobile applications has been established. In this concept, a novel thin-film electrolyte, which separates the cathode from the anode, paved the way to an outstanding high performance thin-film cell concept.

In the present paper the electrolyte development and the manufacturing process is being presented. Within the scope of a systematic basic and development work a highly potential electrolyte structure, consisting of 8YSZ (8 mol.-% Y_2O_3 stabilized ZrO_2), has been developed by using a physical vapor deposition (PVD) gas flow sputtering (GFS) process. Where a standard structure (single-layer configuration) could be established and discussed in detail elsewhere [15], in this work a significant improvement of the electrolyte structure regarding gas-tightness, lesser defect formation and hence higher layer quality has been focused. The scientific approach was assumed that the gas-tightness of the electrolyte can be significantly improved when sequential oxidic and metallic thin-film multi-layers are deposited in an alternated way. This enables generally to interrupt the columnar grain structure during the growth of such thin-film layers. Electrolytes that were fabricated in this way, with two or eight oxide/metal layers and a total thickness of about 4 μm, achieve leakage rates of lesser than 3×10^{-4} hPa dm^3 s^{-1} cm^{-2} (Δp: 100 hPa in air at RT). In contrast, standard electrolyte structures (single layers) possess a leakage rate which is at least a half an order of magnitude higher. Therefore, this novel structure promises a significant improvement of gas-tightness and hence a higher open circuit cell voltage (OCV). The last one is a basic requirement to achieve high cell performances during cell operation. Furthermore, it could be demonstrated that such structures are also highly tolerant with respect to surface flaws and particulate impurities which can occur on the graded anode underground. Finally, electrochemical tests with cells, operating with such a double and multilayer electrolyte system, could be demonstrated, successfully.

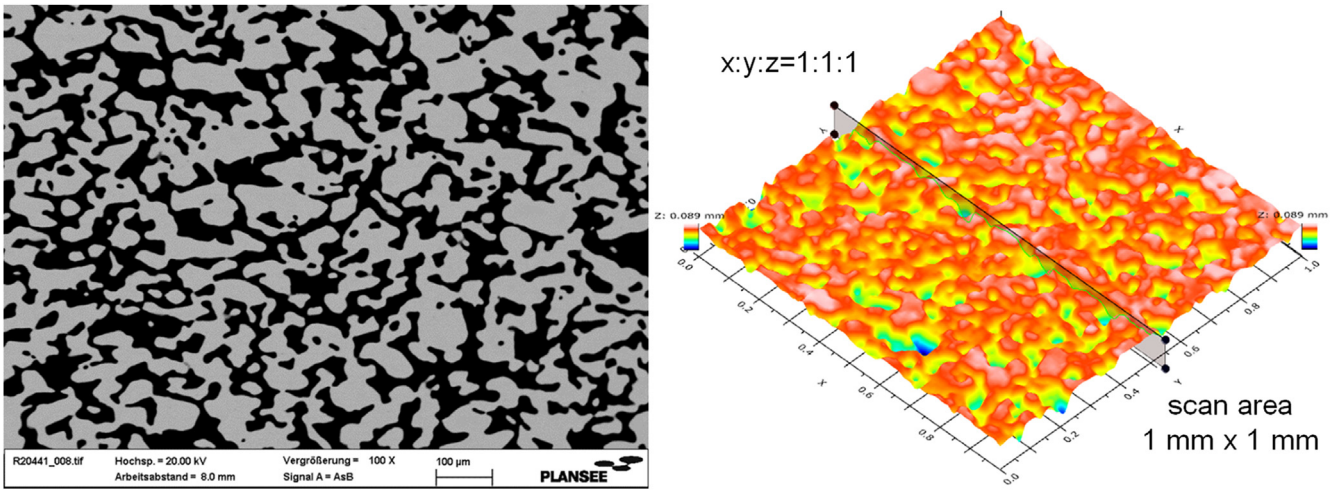

Fig. 2. SEM cross-section of the metallic substrate (left), 3-dimensional optical surface scan of the substrate (x:y:z = 1:1:1, Δz = 0.089 mm) (right) [15].

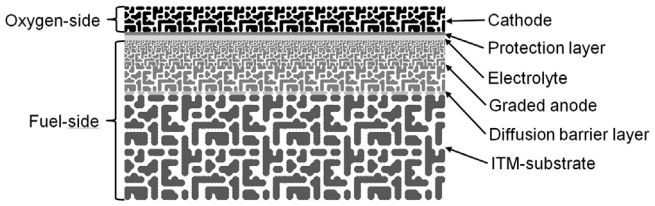

Fig. 3. Schematic cross-section scheme of a metal-supported cell [15].

2. Experimental

2.1. Powder metallurgical manufactured porous substrate

A porous metallic substrate is the backbone of the MSC [13,14]. It ensures the stiffness and the handling of the cell compound and must fulfill the following requirements:

i)It must be highly porous to ensure sufficient gas transport to the anode. The porosity must be stable under long-term operation in reducing atmospheres at temperatures up to 850 °C.
ii)It must be highly creep resistant to ensure long-term structural integrity.
iii)The coefficient of thermal expansion (CTE) of the metallic substrate must match the CTE of the ceramic cell layers as closely as possible.
iv) The electrical conductivity of the substrate must be preserved under long-term operation even at the cathode side where oxide scales can reduce the conductivity significantly.
v) Cr evaporation on cathode side poisons the cathode and must be suppressed.

All requirements are largely fulfilled by an oxide dispersion strengthened (ODS) alloy (Fe26Cr (Mo, Ti), Y_2O_3) [13,14]. An SEM micrograph of the substrate cross section and a 3D topography scan of its surface are shown in Fig. 2.

The porosity of the metallic substrate (thickness: approx. 1 mm; porosity: approx. 40 vol. %) is homogenously distributed over the whole cross section as well as at the surface. Notably, a sufficient fuel gas (H_2, CO…) distribution and supply to the MSC anode, as well as the removal of the exhaust gases (H_2O, CO_2) must be ensured. The subsequent cell layers, particularly the graded anode, can be smoothly deposited as a consequence of the homogeneity of the surface.

2.2. Structure and manufacturing route of metal-supported solid oxide fuel cells

The primary structure of the MSC is a porous metallic substrate with a thickness of ≈1 mm. On top of this backbone, thin-film cell layers are deposited by different procedures. A schematic cross-section of an MSC is shown in Fig. 3.

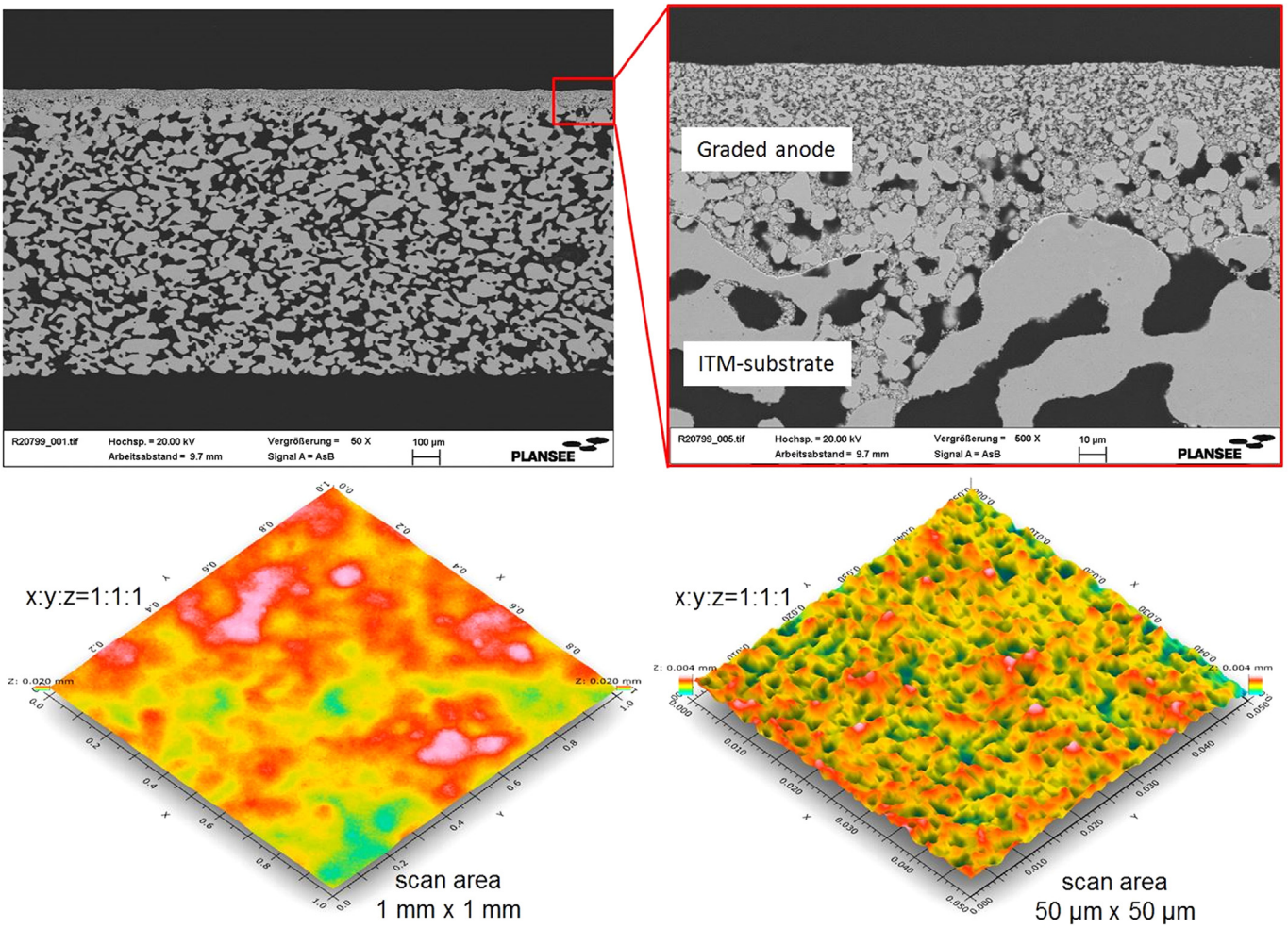

Fig. 4. SEM cross-section of the metallic substrate with graded anode (top) and 3-dimensional optical surface scans of the anode with x:y:z = 1:1:1; scan area 1 mm × 1 mm with Δz = 0.02 mm (bottom left) scan area 0.05 mm × 0.05 mm with Δz = 0.004 mm (bottom right).

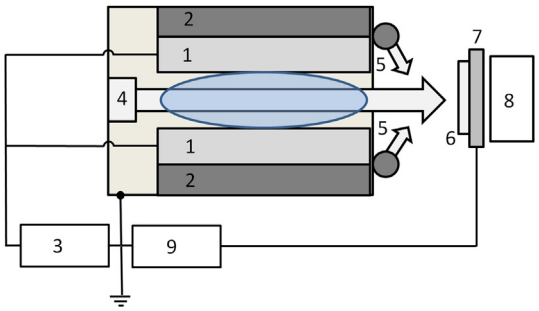

Fig. 5. Cross-section scheme of a GFS-source [20,21].

The manufacturing route of the MSC is as follows:

i) First, a 1–2 μm gadolinium doped ceria (GDC) layer ($Ce_{0.8}Gd_{0.2}O_{2-\delta}$) is placed onto the metallic substrate via magnetron sputtering (reactive sputtering; deposition temperature between 400 °C and 800 °C; metallic $Ce_{0.8}Gd_{0.2}$ targets are used). This GDC constitutes a diffusion barrier layer (DBL) which prevents (i) the diffusion of Ni from the anode into the substrate and (ii) the diffusion of Fe and Cr from the substrate into the anode [16].

ii) Subsequently, an anode composition of 8YSZ (8 mol.-% Y_2O_3 stabilized ZrO_2) and Ni, with a total thickness of 40–70 μm, which features a distinct pore- and grain-size gradient, is applied by screen printing and successive sintering. While the porosity of the starting layer on top of the GDC is coarse, the pore and grain size of the subsequent anode layers decrease gradually so that a very smooth and flat surface is achieved at the top anode layer (pore size distribution on top: approx. 1 μm). Sufficient smoothness and planarity of the anode surface are prerequisites to deposit an electrolyte layer which is both thin and gas-tight. SEM cross-sections of the substrate-anode assembly and scans of the anode surface are shown in Fig. 4.

iii) Then, the electrolyte (8YSZ) with a thickness 4–5 μm is applied by a physical vapor deposition, gas flow sputtering (GFS) process.

iv) On top of the electrolyte a second 1–2 μm thick GDC protective layer ($Ce_{0.8}Gd_{0.2}O_{2-\delta}$) is deposited by magnetron sputtering (reactive sputtering; deposition temperature between 400 °C and 800 °C; metallic $Ce_{0.8}Gd_{0.2}$ targets are used). The function of this layer is to prevent the formation of electrically isolating strontium–zirconium-phases between the electrolyte and the cathode [17–19].

v) Finally, a 20–60 μm porous LSCF ($La_{1-x}Sr_xFe_{1-y}Co_yO_{3-\delta}$) cathode layer is screen printed. The activation and sintering

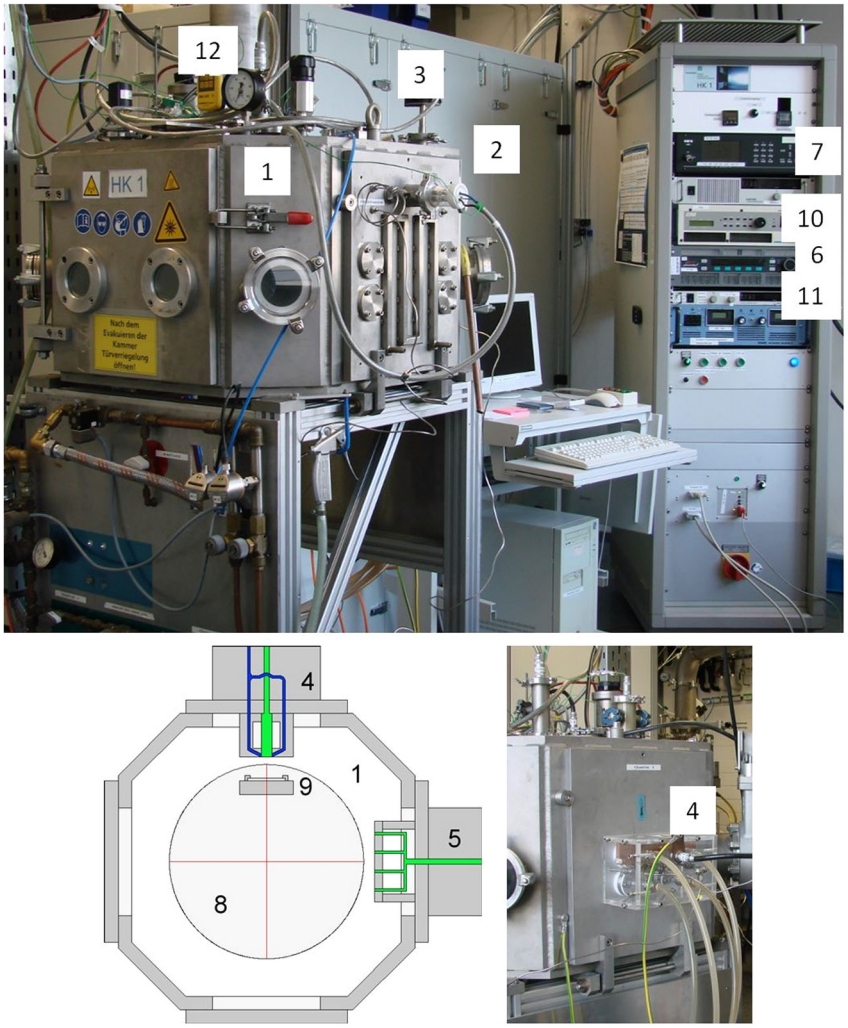

Fig. 6. Gas-flow-sputtering system at Fraunhofer IST in Braunschweig, Germany.

Table 1
Typical electrolyte coating parameters.

Process parameter	Pretreatment	Coating
Inert gas (argon) in sccm	300–500	4000–6000
Reactive gas (O_2) in sccm	0	50–100[a]
Process-pressure in hPa	≈0.1	≈0.5
Source-power in W	0	4000–6000
Bias-voltage in V	≥100	50–150
Duration of process step in min	10	≈15–30
Substrate-temperature in °C	≈500	≈500

[a] The reactive gas is switched on after 10 s (metallic adherent layer).

of the cathode occurs during the start-up of cell/stack operation (operation temperature: 700 °C to 850 °C).

2.3. Production of thin-film electrolytes by a gas-flow sputtering process

A unique physical vapor deposition process (PVD), the "gas-flow sputtering process" (GFS), has many advantages as compared to conventional PVD-sources. Among others there are (i) high deposition rates up to 10 μm h^{-1} and (ii) high process pressures of about 0.5 hPa [20–22], which both foster fast and economic processing. Furthermore, the source design is well adapted for reactive operation conditions so that oxides, carbides and nitrides can be deposited [22].

2.3.1. The gas-flow sputtering source

Fig. 5 shows the cross-section scheme of a GFS-source. The metallic targets (1) are water-cooled (2) and connected to the cathode potential of a source generator (3). The process gas (argon) is fed in at position (4) and flows through the source. At the end of the source, reactive gases (5) can be fed in to grow oxides, nitrides or carbides. The substrate (6) is mounted on the substrate holder (7), which can be moved in front of the source to increase the deposition area. It might be necessary to heat the substrate, e.g. with ceramic heaters (8). To increase the density of deposited layers, the substrate holder can be negatively biased with a pulsed-DC (direct current) generator (9). If sufficient power is supplied and the process pressure is in the right range, the hollow cathode plasma burns between the metallic targets. Target atoms are released from the target by sputtering and transported along with the argon stream onto the substrate.

2.3.2. Setup of the gas-flow sputtering facility

Fig. 6 shows the set-up of a gas flow sputtering system. The octagonal recipient (1) has a volume of about 200 L and 4 door flanges. The pumping speed (2) is ≈1000 m^3 h^{-1}, the chamber pressure is recorded by a capacitance manometer (MKS Baratron® (3)). The linear GFS-sputter source (4) has a length of 250 mm and is flange-mounted horizontally on a door-flange. The pretreatment facility (5) is flange-mounted on a door-flange too. A metallic zirconium-yttrium-alloy (85.2 at.-% Zr, 14.8 at.-% Y) is used as target material to deposit 8YSZ (8 mol.-% Y_2O_3 stabilized ZrO_2) in the reactive mode. A pulsed-DC generator (6) is applied as source generator (Pinnacle Plus, Advanced Energy) which supplies the source in DC-mode. The process and reactive gas supply is guaranteed by a gas flow regulation system (MKS, Multi-Gas Controller 647B (7)). The substrate movement is realized by a turntable (8) onto which the substrate holder is mounted (9). A multiphase motor enables the positioning and the oscillation movement during the coating process. A mid frequency bias-voltage is applied on the substrate holders via an MF-Plasma-Generator (ENI, RPG-50, 5 kW Puls-DC) (10). This mid frequency bias-voltage (200 kHz, duration of pulse: 1 μs) enables the coating of non-conducting layers as e.g. oxides. The substrate is heated by ceramic heaters which are fed by a Xantrex XRF 300-9 power supply (11) and the temperature is measured on the substrate holder directly by thermocouples (12).

2.3.3. Process control and typical coating parameters of thin film GFS-electrolytes

First the work piece (metallic substrate (≈1 mm) with GDC diffusion barrier layer (1–2 μm) and anode (40–70 μm)) is fixed on the substrate holder, then the recipient is evacuated and the part is

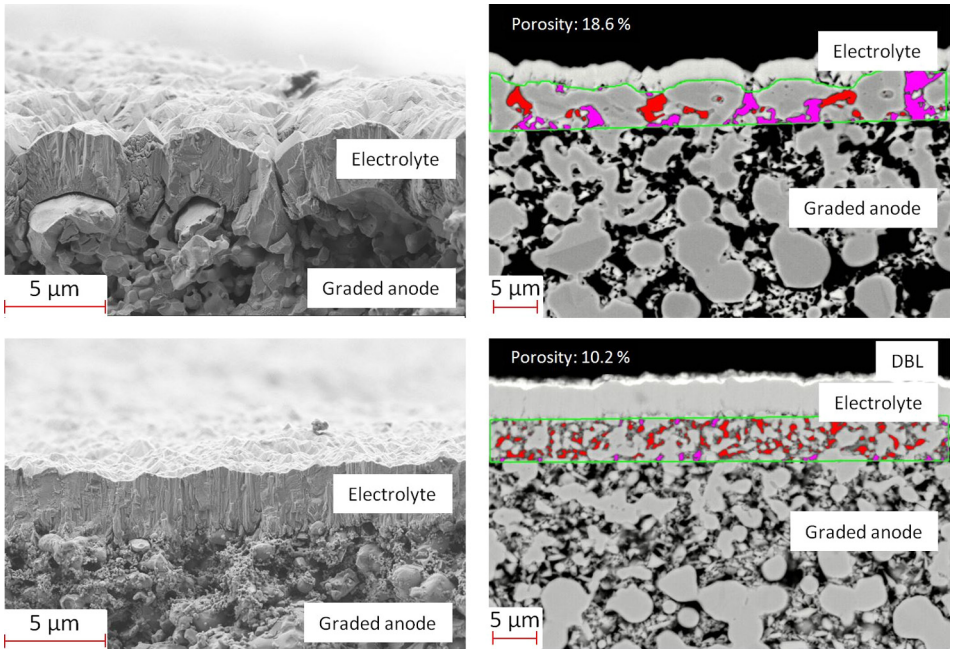

Fig. 7. SEM cross-sections: fracture surfaces (left) and polished cross-section with marked pores (right) of two anode structures which were electrolyte-coated simultaneously. Coarse anode structure (AV3) (top), fine anode structure (AV6) (bottom).

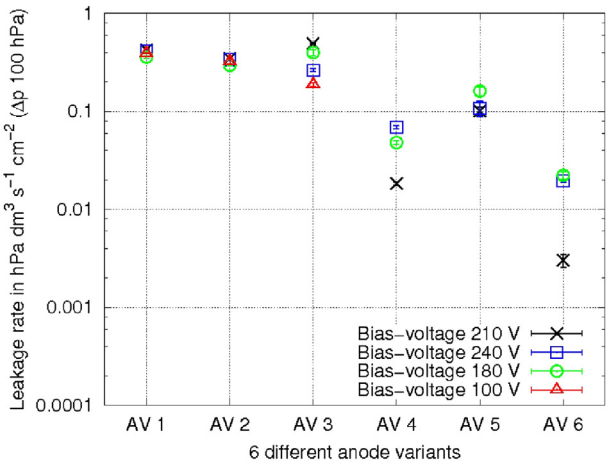

Fig. 8. Leakage rates of four electrolyte coating processes (various bias-voltages) on six anode variants (AV1–AV6).

heated. Next, it is pretreated by applying a bias-voltage (mid frequency, 200 kHz, duration of pulse: 1 μs) on the substrate holder until a glow discharge arises, which activates the substrate surface (see Table 1). Subsequently, the GFS-source is turned on and the substrate holder commutes in front of the source to enable the coating of large areas. During the first seconds of electrolyte processing, the reactive gas feeding is disabled (no O_2) to deposit a very thin metallic adherent layer (estimated to 30 nm) between the anode and the electrolyte which should improve adhesion. Table 1 summarizes typical pretreatment and process parameters of GFS-electrolyte coatings.

The pressure is adjusted by an argon gas flow which enables a hollow cathode glow discharge. With reactive gas flow rates of 50–100 sccm, O^{2-} conductive 8YSZ layers can be deposited from the metallic zirconium–yttrium targets. Based on typical coating parameters shown in Table 1, three different electrolyte configurations were developed [23,24]:

i) Single-layer electrolyte: It is applied in reactive mode with 50–100 sccm O_2, so that a continuous 8YSZ electrolyte with a typical thickness of 3–5 μm is generated.
ii) Double layer electrolyte: The first layer (3–5 μm) of the electrolyte is sputtered in reactive mode (50–100 sccm O_2) and subsequently a thin top layer (300–500 nm) is deposited in metallic mode (no O_2). Unexpectedly, the discontinuity between the oxide base-layer and the metallic top-layer promoted the gas-tightness of the entire electrolyte. However, since the metallic layer cannot conduct O^{2-}-ions, the electrolyte must be heat-treated (≈500 °C) in an oxygen-containing atmosphere to finally transform the metallic film into 8YSZ. That transformation occurs during the start-up of cell/stack operation (operation temperature 700 °C–850 °C).
iii) Multi-layer electrolyte: The electrolyte consists of a sequence of 8 thin layers (300–500 nm) which are sputtered alternately in metallic (no O_2) and reactive (50–100 sccm O_2) mode. The resulting electrolyte structure further improves the gas-tightness of the assembly, especially less addicted to the underground structure. Again, the metallic layers are transformed into 8YSZ during the start-up of cell/stack operation.

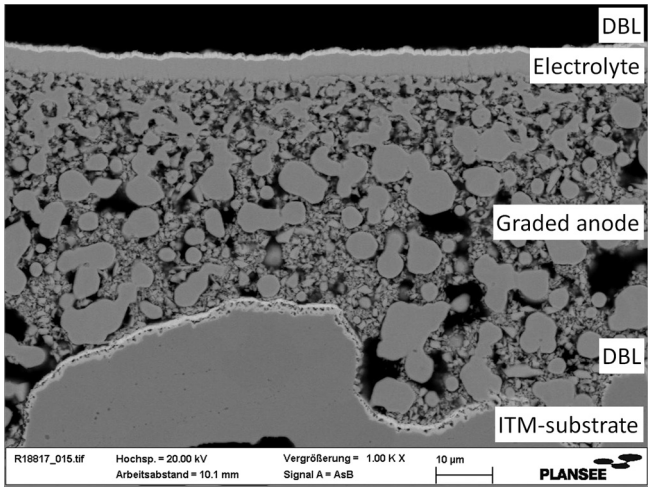

Fig. 9. State of the art MSC (type: MSC06b) without cathode layer.

A key quality criterion of an MSC is its electrolyte performance. Firstly, the electrolyte must safely separate the anode from the cathode side to ensure high open cell voltages (OCV) [25–27]. Secondly, reduction of internal impedance demands electrolytes to be as thin as possible to ensure high power densities [28,29].

To compare the gas-tightness of electrolytes, leakage-rates were carefully assessed. The measurement set-up is as follows: vacuum is applied on a sealed electrolyte surface area and the pressure increase is recorded. In this paper the leakage-rate is reported in hPa dm^3 s^{-1} cm^{-2} at a pressure difference of 100 hPa ("air leak rate") [30].

2.4. Electrochemical characterization methods

Initial electrochemical characterizations of two MSCs with single-layer electrolyte, two MSCs with double-layer electrolyte and one MSC with multi-layer electrolyte (compare with Fig. 11) were performed at Karlsruhe Institute of Technology. LSCF has been used as cathode material and the active cell-layer area was 1 cm^2. The operation temperature was 850 °C and 250 nccm H_2 was fed to the anode and 250 nccm air was fed to the cathode side.

3. Results

3.1. Anode impact on the GFS-electrolyte

As discussed in Chapter 2.2, the anode and the cathode of the MSC are separated by a thin-film 8YSZ electrolyte. Firstly a graded anode structure (8YSZ and Ni) is deposited onto the metallic substrate (1 mm thick FeCr–ODS alloy, approx. 100 μm pore size, coated with a 1 μm diffusion barrier layer ($Ce_{0.8}Gd_{0.2}O_{2-\delta}$)) to reduce the pore-size at the anode surface [23,24]. This is the prerequisite to allow an effective sealing of the porous anode by a gas-tight thin-film GFS-electrolyte [15,23,24]. Initially, six different graded anodes with various porosity and particle size distributions were developed and the growth behavior of the GFS thin-film electrolyte was examined in reactive deposition mode of the GFS-source (50–100 sccm O_2, single-layer electrolyte) [23]. To compare the six anodes, they were coated at the same time in the similar process using the process parameters from Table 1. Fig. 7 shows the SEM images of two anode variants with as-deposited electrolytes.

The left side of Fig. 7 displays SEM micrographs of fracture surfaces and on the right side the corresponding polished cross sections are shown. The microstructures of the two anodes differ strongly, i.e. the anode AV3 (top) features coarse particles and pores and is generally less homogeneous than the anode AV6 (bottom).

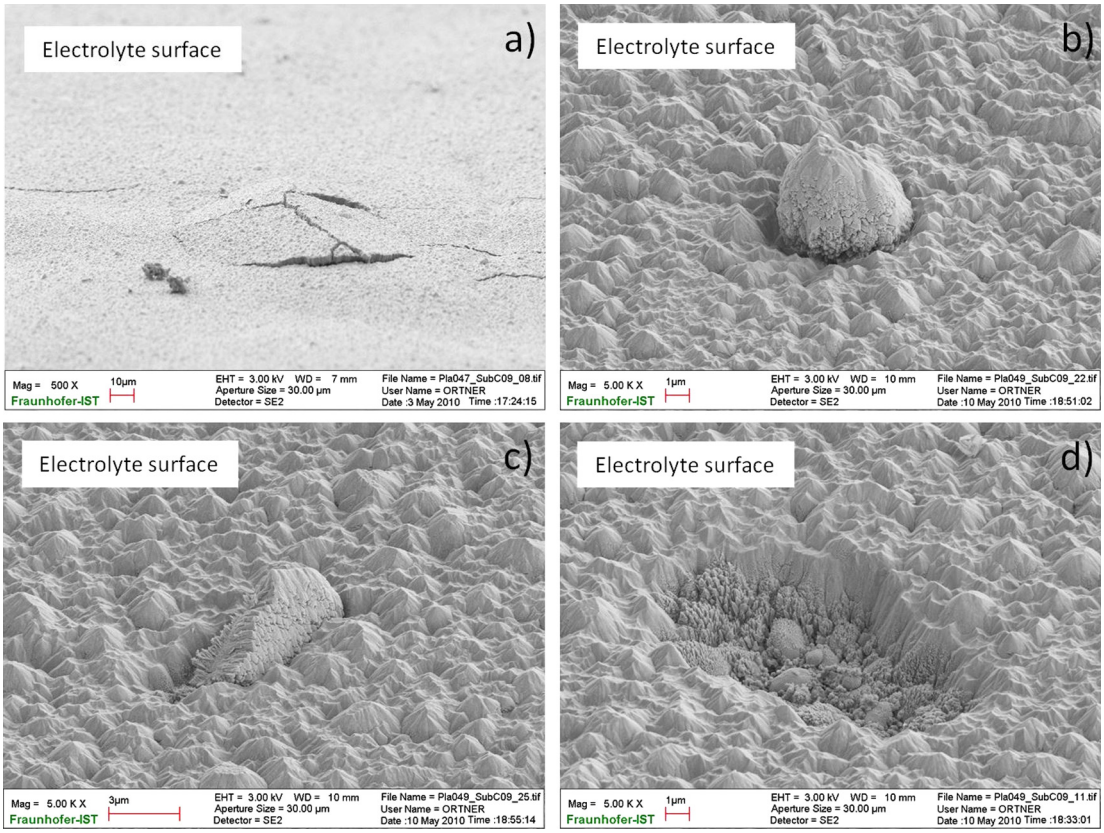

Fig. 10. Typical electrolyte coating defects; bulges and spallation (a), nodular growth (b), accretion growth (c), outburst (d). Note the different magnifications of (a) and (b–d).

Obviously, the morphology of the GFS-electrolytes is strongly influenced by their corresponding anode surface topography, demonstrating that the latter structure is crucial for the performance of the coating. Later it will be shown that the coating sequence is another decisive processing element, which nevertheless builds decisively on a well prepared anode surface.

One major goal in MSC-development is to manufacture cells with an electrolyte as thin as possible [25,29]. Notably, a thickness of 4–5 µm is far too thin to create gas-tight electrolytes on the coarse AV3 anode structure (Fig. 7 top), whereas the gas tightness of the fine anode structure AV6 (Fig. 7 bottom) is acceptable at that thickness level.

Fig. 8 compares the leakage rates of four electrolyte modifications (different bias-voltages) which were deposited onto six different anode variants. Again, all anode variants were processed simultaneously. Notably, the anode structure impacts the gas permeability significantly, more than the bias-voltage (mid frequency, 200 kHz, duration of pulse: 1 µs). The leakage rate of anode AV6 in Fig. 7 (bottom) is, depending slightly on the bias-voltage, almost two orders of magnitude lower than of the AV3 anode in Fig. 7 (top). Hence, a fine-grained, homogenous and flat anode surface leads to electrolytes which safely separate the anode from the cathode gases.

Fine-tuning of the electrolyte microstructure becomes feasible through the bias voltage. Based on the results for AV6, coated with a 4 µm electrolyte (reactive mode; 50–100 sccm O_2, adapted bias-voltage), MSCs suitable for electrochemical characterization can be produced. Fig. 9 shows a cross-section of an optimized MSC half-cell (without cathode layer), which already contains a 1 µm thin-film GDC diffusion barrier layer on top. With the optimized MSCs in Fig. 9 leakage rates of 2.10^{-4} hPa dm^3 s^{-1} cm^{-2} (Δp: 100 hPa, 22.3 cm^2 measurement area, room temperature) were obtained. From a geometric point of view it appears feasible to seal the AV6 anode structure with an even thinner electrolyte. However, experiments demonstrated that the AV6 anode requires at least a 4 µm single-layer electrolyte to obtain sufficient gas tightness.

3.2. Flaws in the electrolyte

Beside the dominant impact of the anode structure on the gas-tightness of the electrolyte, coating defects as well as impurities of the anode surface finally control the integrity of the electrolyte [31]. Fig. 10 depicts representative coating flaws in thin-film electrolytes. The spallation in Fig. 10a results from high residual compression in the electrolyte layer. Driven by these stresses (approx. 0.5–1.5 GPa, measured by XRD), the electrolyte buckles with the fracture origin being either a delamination at the anode–electrolyte interface or a crack in the anode structure.

Gas-tight single-layer electrolytes can be manufactured by using high bias-voltages on the one hand and thick electrolytes on the other hand. Both parameters stress the substrate and at a certain point the typical failures are shown in Fig. 10, occur [32]. Therefore a compromise between electrolyte thickness, bias-voltage and leakage rate is mandatory to manufacture large-area, defect-free MSCs.

As already pointed out in Chapter 3.1, the integrity of the electrolyte depends mainly on the surface structure of the graded anode. If, moreover, particulate impurities are also present at the anode surface, nodular defects can occur [33–35]. Examples for such flaws are shown in Fig. 10b and c. The nodules are more or less strongly bonded to the surrounding electrolyte and will be typically pulled above a certain layer thickness threshold. In that case cavities are left behind the pulled-out nodule as illustrated in Fig. 10d. Evidently, embedded flaws increase the leakage rate less than cavities, because the latter weaken the electrolyte morphology even more.

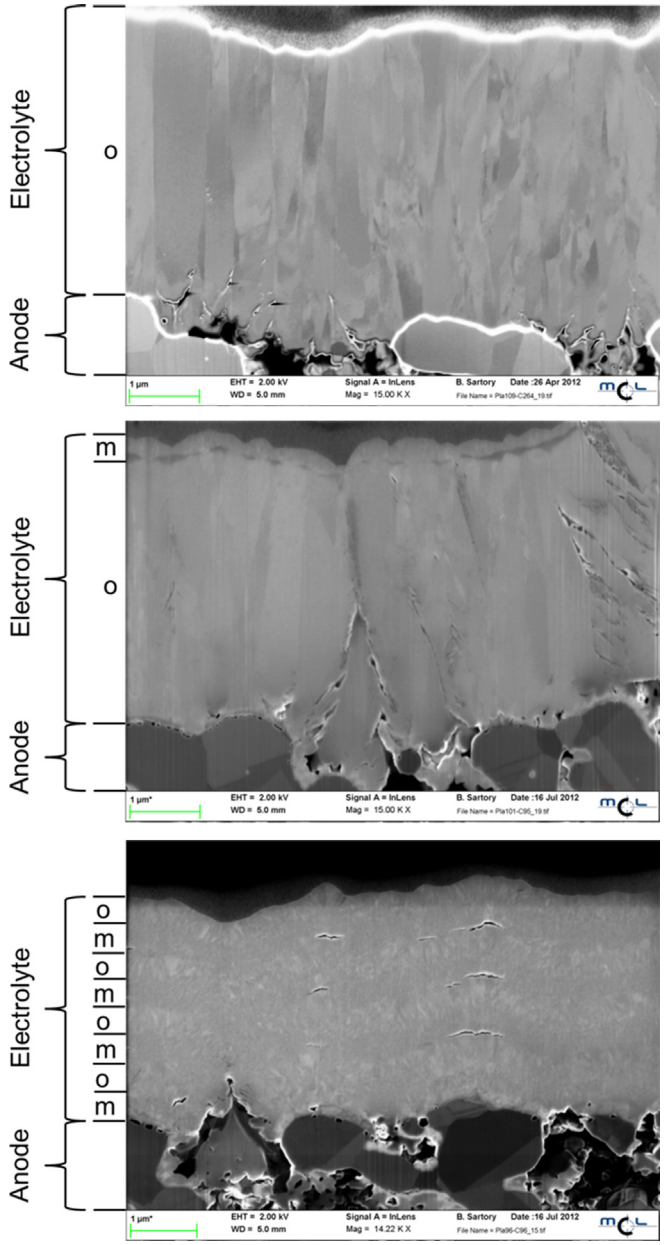

Fig. 11. Different electrolytes comprising reactive and metallic layers [metallic layers (m), oxide electrolyte layers (o)]; 4 μm pure oxide electrolyte (top); 3.5 μm oxide layer with 0.5 μm metallic top layer (center); electrolyte compound of four 0.5 μm metallic and four 0.5 μm oxide layers (bottom).

Accordingly, a dust free environment is mandatory during manufacturing of the anode to avoid nodular defects as effectively as possible. As discussed in Chapter 2.2, the anode is applied by multi-layer screen printing followed by a sintering process. To this end, the screen printing paste must be very homogeneous to avoid local inhomogeneity at the anode surface which could disturb the integrity of gas-tight electrolytes or raise the required electrolyte thickness. The influence of the anode structure on the required electrolyte thickness and the influence of surface impurities were examined by a numerical simulation and will be discussed in a forthcoming paper.

3.3. Electrolyte structures

As shown above, it is the pore size distribution (approx. 1 μm) and the homogeneity of the anode surface which control the microstructure and the integrity of the growing electrolyte. Nevertheless, if flaws and particulate impurities are present at the anode surface, they are reproduced in the electrolyte structure and may generate flaws as well. To reduce these impacts, the layered electrolyte structures can be deposited either by

(i) Sputtering of a separate 300–500 nm metallic film (no O_2 addition) on top of the initial 3–5 μm thick oxide layer (50–100 sccm O_2) or
(ii) Applying a series of alternating 300–500 nm metallic (no O_2 addition) and reactive oxide (50–100 sccm O_2) thin films.

Fig. 11 displays SEM images of three horizontally layered electrolyte configurations. The electrolyte in the top SEM image of Fig. 11 contains a 4 μm single oxide layer (2×10^{-4} hPa dm^3 s^{-1} cm^{-2}), the electrolyte in the center comprises a two-layer electrolyte with a 3.5 μm oxide and on top a 0.5 μm thick metallic film (8×10^{-4} hPa dm^3 s^{-1} cm^{-2}), and finally a multi-layer electrolyte in the bottom of Fig. 11 is made up of eight alternating 0.5 μm metallic and 0.5 μm oxide films (3×10^{-4} hPa dm^3 s^{-1} cm^{-2}). The leakage rates were measured at Δp of 100 hPa, a measurement area of 22.3 cm^2 and room temperature. Obviously, switching from the metallic to the reactive deposition mode (or vice versa), triggers a change in the electrolyte's morphology.

Firstly it should be noted that, as the crystallite growth is interrupted after each layer, the grain size of that layer is confined to the particular layer thickness. Consequently, the columnar 8YSZ crystals in a single layer electrolyte extend from the anode to the cathode interface. The recurring layer structure however, breaks up the columnar structure, as new crystals grow in each layer. This morphology suppresses the development of potential flaws along the columnar grains of pure single-oxide electrolytes and, consequently, improves the gas tightness of the electrolyte. Based on different thermal expansion coefficients between metallic and oxidic layers, micro cracks can occur in the multi-layer-electrolyte, parallel to anode and cathode layer, and might reduce the compound stability marginally. These cracks do not influence the leakage rate negatively; since they do not spread from anode to cathode side directly (see in Fig. 11). Thus, by introducing layered electrolytes it is feasible to seal porous anode structures more effectively.

3.4. Electrochemical characterization of MSCs

The electrical characteristics of MSCs are presented in Fig. 12, which plots the cell voltages and cell temperatures as a function of

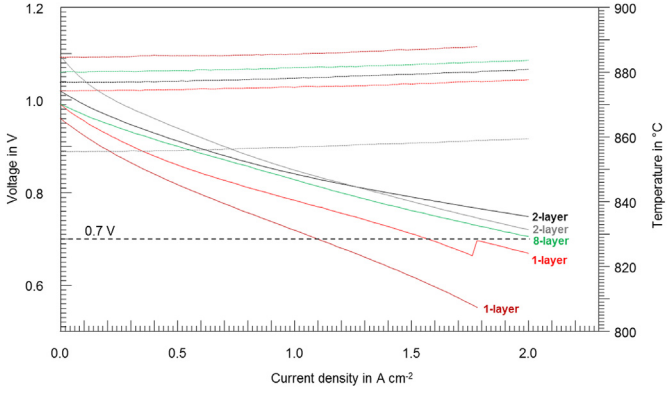

Fig. 12. Electrochemical characterization of two MSCs with single-layer electrolyte, two MSCs with double-layer electrolyte and one MSC with multi-layer electrolyte (Fuel gas: 250 nccm H_2; Oxide gas: 250 nccm air; 850 °C; 1 cm^2 measurement area).

current density. The *I–V*-characteristics have been measured at 850 °C with 250 sccm H_2 on anode and 250 sccm air on cathode side at an measurement area of 1 cm^2. The open cell voltage (OCV; 0 A cm^{-2}) indicates the gas-tightness of the electrolyte. MSCs with 2-layer electrolytes show the best OCV performance and single-layer electrolyte MSCs are considerable worse. Nonetheless the MSC with the 8-layer electrolyte shows a non-distinguish OCV in between. The large spreading of the OCV values can be explained by quality discrepancies in the anode manufacturing through surface defects or surface contaminations in that phase of MSC development. However, MSCs with double or multilayer-electrolyte show better values in average. At a cell voltage of 0.7 V MSCs with single layer electrolyte show a current density of approximately 1.1 A cm^{-2} respectively 1.6 A cm^{-2}, whereas all three multilayer electrolyte MSCs show a much higher performance of more than 2 A cm^{-2} (the test rig is confined to 2 A cm^{-2}). Based on this electrochemical characterization results it is assumed that the multilayer-electrolyte MSCs exhibit a better tightening behavior compared to single-layer-electrolyte MSCs. To glory in the advantages of multi-layer electrolytes the homogeneity of the (sintered) anode surface must be further raised to obtain an ideal gastight anode–electrolyte composite and a good long-term stability of the MSC.

4. Conclusions

Starting from a porous P/M Fe–Cr-substrate, a metal supported cell was developed successfully. The key feature of this MSC is a gas-tight and well adherent thin-film electrolyte which was deposited by gas flow sputtering (GFS). To achieve sufficiently low leakage rates, an electrolyte thickness >4 μm is required. Analysis of SEM images reveal, that defects and particulate impurities at the anode surface or of the anode itself raise the required electrolyte width and explain why the actually observed 4 μm film thickness threshold is needed. Depositing electrolyte structures with alternating reactive oxidic and metallic layers significantly improves the impermeability of the electrolytes and, simultaneously, reduces the effects of anode surface flaws and particles. Finally, electrochemical characterizations of single layer electrolyte MSCs, double-layer electrolyte MSCs and multilayer electrolyte MSCs are presented. It was shown that the double or multi-layer electrolyte MSCs show a higher open cell voltage (in average) and a higher cell performance than single-electrolyte-layer MSCs. At an operation temperature of 850 °C, the double or multi-layer-electrolyte MSCs show a current density of more than 2 A cm^{-2} @ 0.7 V. This indicates the substantial potential of this MSC-types for mobile applications, e.g. for the electrical power supply in SOFC truck auxiliary power units.

Acknowledgments

The authors would like to acknowledge Dr. Andre Weber (Karlsruhe Institute of Technology) for the electrochemical characterization of the MSCs.

References

[1] N.H. Menzler, F. Tietz, S. Uhlenbruck, H.P. Buchkremer, D. Stöver, J. Mater. Sci. 45 (2010) 3109–3135.
[2] www.bloomenergy.com, November 2013.
[3] R.J. Payne, J. Love, M. Kah, in: "CFCL's BlueGen Product" Proceedings of Solid Oxide Fuel Cell, Montreal, 2011, pp. 81–85. S. Singhal, K. Eguchi, SOFC-XII.
[4] N. Christiansen, H. Holm-Larsen, S. Primdahl, M. Wandel, S. Ramousse, A. Hagen, ECS Trans., 35, 2011, in: Proceedings of the SOFC-XII SYMPOSIUM at the 219th ECS Meeting, Montreal, Canada, 1 to 6 May 2011.
[5] G. Schiller, T. Franco, R. Henne, M. Lang, R. Ruckdäschel, P. Otschik, K. Eichler, in: Proceedings of the 7th International Symposium on Solid Oxide Fuel Cells (SOFC-VII), ECS Proceedings, vol. 2001-16, 2001, pp. 885–894.
[6] Th. Franco, R. Mücke, M. Rüttinger, N. Menzler, L.G.J. de Haart, Andreas Venskutonis, in: P. Connor (Ed.), Proceedings of 9th European Solid Oxide Fuel Cell Forum, 2010, pp. 16–20. Lucerne, Switzerland.
[7] A. Venskutonis, G. Kunschert, E. Mueller, H.-M. Höhle, ECS Trans. 7 (1) (2007) 2109–2115, http://dx.doi.org/10.1149/1.2729325. The Electrochemical Society.
[8] Th. Franco, R. Henne, in: S.C. Singhal, M. Dokiya (Eds.), Solid Oxide Fuel Cells VIII (SOFC-VIII), Hrsg, Electrochemical Society, Pennington, NJ, 2003, pp. 923–932.
[9] G. Kunschert, K.H. Kailer, S. Schlichtherle, G.N. Strauss, in: Proceedings of 8th European SOFC Forum, Lucerne/Switzerland, July 2008.
[10] Th. Franco, K. Schibinger, Z. Ilhan, G. Schiller, A. Venskutonis, in: K. Eguchi, S.C. Singhal, H. Yokokawa, J. Mitzusaki (Eds.), Solid Oxide Fuel Cells X (SOFC-X) – Part 1, vol. 7, 2007, ISBN 978-1-56677-555-7, pp. 771–780 no. 1.
[11] M. Rüttinger, R. Mücke, Th. Franco, O. Büchler, N.H. Menzler, A. Venskutonis, in: Proceedings of the Solid Oxide Fuel Cell, Montreal, 2011, pp. 259–269. S. Singhal, K. Eguchi, SOFC-XII.
[12] J. Rechberger, P. Prenninger, SAE Technical Paper Series 2007-01-4273, World Congress, Detroit, 2007.
[13] A. Venskutonis, G. Kunschert, M. Brandner, T. Franco, F. Jansen, Recent Progress in Powder metallurgical "Ready to Stack" Interconnect Components for various SOFC Applications, A0906, Abstract 220, Oral Presentation, Interconnects and Coatings, 2008.
[14] B. Tabernig, Th. Franco, A. Venskutonis, H. Kestler, L.S. Sigl, in: Proceedings, EURO PM 2011, Barcelona, Spain, 2011.
[15] M. Haydn, T. Franco, R. Mücke, M. Rüttinger, N.H. Menzler, A. Weber, A. Venskutonis, L.S. Sigl, A Novel Manufacturing Route for Metal Supported Thin-Film Solid Oxide Fuel Cells, PM-2012, Yokohama, Japan.
[16] M.C. Tucker, J. Power Sources 195 (2010) 4570–4582.
[17] H. Yokokawa, N. Sakai, T. Horita, K. Yamaji, M.E. Brito, H. Kishimoto, J. Alloys Compd. 452 (2008) 41–47.
[18] S. Uhlenbruck, N. Jordan, D. Sebold, H.P. Buchkremer, V.A.C. Haanappel, D. Stöver, Thin Solid Films 515 (2007) 4053–4060.
[19] H. Yokokawa, H. Tu, B. Iwanschitz, A. Mai, J. Power Sources 182 (2008) 400–412.
[20] S. Tang, U. Schulz, Surf. Coat. Technol. 204 (2009) 1087–1091.
[21] K. Ortner, M. Birkholz, Th. Jung, Vak. Forsch. Prax. 15 (5) (2003) 236–239.
[22] Th. Jung, T. Kälber, V.v.d. Heide, Surf. Coat. Technol. 86–87 (1996) 218–224.
[23] M. Haydn, Entwicklung und Herstellung von metallgestützten Festelektrolyt-Brennstoffzellen mit Hilfe des Hohlkathoden-Gasflusssputterns, vol. 180, Diss., Bochum, Univ.,, 2013, ISBN 978-3-89336-886-0, p. D294. Ph.D. Work, Schriften des Forschungszentrums Jülich – Energy and Environment.
[24] M. Haydn, K. Ortner, Th. Franco, N.H. Menzler, A. Venskutonis, L.S. Sigl, Development of Metal Supported Solid Oxide Fuel Cells Based on Powder Metallurgical Manufacturing Route, vol. 3, EuroPM, Sweden Gothenburg, 2013, pp. 162–170. Metal Supported Membranes.
[25] P.S. Devi, A.D. Sharma, H.S. Maiti, Trans. Indian Ceram. Soc. 63 (2) (April–June 2004) 75–98.
[26] M. Liu, M.E. Lynch, K. Blinn, F.M. Alamgir, Y. Choi, Mater. Today. ISSN: 13697021 14 (11) (2011) 534–546. Elsevier Ltd.
[27] N.Q. Minh, J. Am. Ceram. Soc. 76 (3) (1993) 563–588.
[28] O. Yamamoto, Electrochim. Acta (2000) 2423–2435.
[29] S.C. Singhal, K. Kendall, High Temperature Solid Oxide Fuel Cells: Fundamentals, Design and Applications, Elsevier Ltd., 2003, ISBN 1856173879, pp. 197–225 pages 1-17, 83-91.
[30] Th. Franco, Entwicklung und Charakterisierung von anodenseitigen Diffusionsbarriereschichten für metallgetragene oxidkeramische Festelektrolyt-Brennstoffzellen, Ph.D. Work, German Aerospace Center, Stuttgart, Germany, 2009, pp. 63–64.
[31] N. Jordan Escalona, Energy Environ., Herstellung von Hochtemperatur-Brennstoffzellen über physikalische Gasphasenabscheidung; Schriften des Forschungszentrums Jülich, vol. 32, 2009, ISBN 978-3-89336-565-4
[32] R.W. Knoll, E.R. Bradley, Thin Solid Films 117 (1984) 201–210.
[33] X. Liu, D. Li, Y. Zhao, X. Li, Appl. Opt. 49 (10) (April 2010).
[34] K.H. Guenther, Appl. Opt. 20 (6) (March 1981).
[35] R. Mattheis, F. Thrum, H.-J. Anklam, Thin Solid Films 188 (1990) 335–340.